Complex magnetic order in the Nd(Tb)Fe₃(BO₃)₄ multiferroic revealed by single-crystal neutron diffraction

I. V. Golosovsky,[1,*] A. I. Vasilev,[1] A. A. Mukhin,[2] E. Ressouche,[3] V. Skumryev,[4] I. Urcelay-Olabarria,[5] I. A. Gudim,[6] and L. N. Bezmaternykh[6]

[1]*National Research Center "Kurchatov Institute", B.P. Konstantinov Petersburg Nuclear Physics Institute, 188300, Gatchina, Russia*
[2]*Prokhorov General Physics Institute, RAS, 119991, Moscow, Russia*
[3]*Université Grenoble Alpes, CEA, INAC-MEM, 38000, Grenoble, France*
[4]*Institució Catalana de Recerca i Estudis Avancats, E-08010 Barcelona, Spain*
[5]*Fisika Aplikatua II, Zientzia eta Teknologia Fakultatea, Universidad del País Vasco, UPV/EHU, 48940, Bilbao, Spain*
[6]*Kirenskii Institute of Physics, Siberian Division of RAS, 660038, Krasnoyarsk, Russia*

Magnetic structure of the substituted multiferroics-ferroborates $Nd_{0.9}Tb_{0.1}Fe_3(BO_3)_4$ and $Nd_{0.8}Tb_{0.2}Fe_3(BO_3)_4$ were determined in the framework of a self-consistent refinement of the single crystal neutron diffraction data. The small substitution of Nd for Tb leads to the reorientation of the main antiferromagnetic vector **L** from the basal plane towards the hexagonal axis. The reorientation takes place via an angular structure for which **L** does not coincide with the principal crystallographic directions and evolves with temperature due to competing magnetic anisotropies of Fe, Nd, and Tb subsystems. Our refinement at 2 K reveals the existence of distortions in the collinear antiferromagnetic Fe spin arrangement suggested before in other ferroborates. Therefore, besides the main antiferromagnetic vector **L**, the magnetic structure involves additional fine symmetrized combinations of spin components allowed by symmetry. They coexist with certain **L** components and could originate from the antisymmetric Dzyaloshinsky-Moriya Fe-Fe exchange interactions. At higher temperatures, the magnetic structure is described by the simple collinear model, where the **L** vector is deviated from the hexagonal plane.

I. INTRODUCTION

Rare-earth ferroborates $ReFe_3(BO_3)_4$, a new class of non-centrosymmetric multiferroics with a rhombohedral structure of the huntite mineral [1], have attracted considerable attention [2,3]. The interest in these multiferroics is caused by the discovery of the strong dependence of the electric polarization on the magnetic field, which is important for practical applications [4,5]. Ferroborates also demonstrate interesting magnetic phenomena since they contain two strongly interacting magnetic subsystems: rare earth and iron sublattices. The latter leads to a complex magnetic behavior, which is governed by the balance between the magnetic interactions.

A characteristic feature of these compounds is the combination of the crystalline anisotropy of the iron sublattice, caused by the chains of Fe^{3+} ions along the hexagonal axis and the rare earth single-ion anisotropy. The rare-earth ions are relatively far apart, their interaction is weak, and the intrinsic magnetic order in rare earth sublattice does not take place down to very low temperatures. Therefore, below the Néel temperature $\sim$30–35 K the magnetic order in the rare-earth sublattice is induced by the iron sublattice.

There are two types of the antiferromagnetic order in these compounds: the *"easy-plane"* type (Re = Ce, Nd, Er) [6–9], when the Fe spins lie in the basal plane, perpendicular to

the trigonal axis and the *"easy-axis"* type, with spins aligned along the trigonal axis (Re = Pr, Tb, Dy) [9–11] (Fig. 1).

The magnetoelectric properties of ferroborates depend on the rare-earth ions, primarily, because of divers anisotropy of the rare-earth ion and the strong Re-Fe exchange interaction. It is important to note a fundamental circumstance: The spontaneous electric polarization appears only in the *"easy-plane"* state, although the magnetic field can induce polarization in the *"easy-axis"* state too.

In contrast to manganites with centrosymmetric crystal structure, where the electric polarization is determined by an incommensurate cycloidal magnetic order which breaks the inversion symmetry [12,13], in ferroborates the crystal structure is noncentrosymmetric and the electric polarization is induced by an antiferromagnetic order or by the external magnetic field.

In this work, we present a single crystal neutron diffraction study of the magnetic order in the substituted system: $Nd_{1-x}Tb_xFe_3(BO_3)_4$ with $x = 0.1$ and $x = 0.2$. In the outermost compound $NdFe_3(BO_3)_4$ at low temperatures an incommensurate magnetic structure was observed, which transforms into collinear, *"easy-plane"* type magnetic order slightly above 13 K [7,8,14]. In the other outermost compound $TbFe_3(BO_3)_4$, the magnetic order is of *"easy-axis"* type [10].

Nd^{3+} has a prolate 4f-charge distribution and positive second-order Stevens coefficient, while Tb^{3+} has an oblate charge distribution and negative Stevens coefficient. A strong difference in the magnetic structures due to the competition
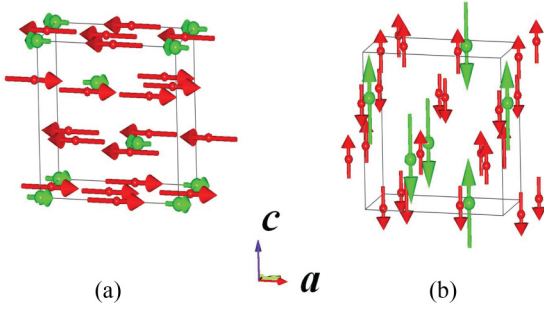
*golosovsky_iv@pnpi.nrcki.ru

FIG. 1. Magnetic structures for the utmost compounds $NdFe_3(BO_3)_4$ [7] (a) and $TbFe_3(BO_3)_4$ [10] (b) are shown. Rare earth moments are shown in green, iron spins in red.

of the different single-ion anisotropies suggests a complex magnetic structure in the mixed compositions, which is a subject of our research. Hence, intermediate compositions such as $Nd_{1-x}Tb_xFe_3(BO_3)_4$ are interesting for elucidating the role of the rare earth single-ion anisotropy in the setting of a given magnetic structure.

Preliminary magnetic measurements demonstrated that the magnetic structure becomes uniaxial, similar to $TbFe_3(BO_3)_4$ already at 20% of Tb. Therefore, we explored the samples with $x = 0.1$ and $x = 0.2$ compositions.

II. EXPERIMENT

The single crystal neutron diffraction experiments were carried out at the diffractometer D15 in the Institute Laue-Langevin (Grenoble, France) with a neutron wavelength of 1.172 Å.

We used mm-size single crystals with nominal composition $Nd_{0.9}Tb_{0.1}Fe_3(BO_3)_4$ and $Nd_{0.8}Tb_{0.2}Fe_3(BO_3)_4$ prepared at the Institute of Physics in Krasnoyarsk. The crystals were enriched with the isotope ^{11}B to decrease neutron absorption. They were mounted inside the so-called *"Displex"* cryostat, providing sample temperatures in the temperature range 1.5–300 K and allowing measuring of a large number of reflections.

In order to check for phase separation, which is possible for the doped compounds due to inhomogeneous distribution of Tb and Nd ions, the profiles of (0 0 −3) and (0 −3 0) nuclear reflections were measured with the same resolution and compared with those for pure $NdFe_3(BO_3)_4$. No phase separation was detected within of our experimental resolution (see Supplemental Material [15]).

The diffraction patterns were analyzed using the FULL-PROF SUITE package [16]. Because the single crystals were rather large and had an irregular shape, the refinement of the magnetic structure parameters included the correction for anisotropic extinction. Scale factor was refined from the nuclear reflections and it was fixed in the magnetic refinement.

III. FEATURES OF THE MAGNETIC AND CRYSTAL STRUCTURES

A. Crystal structure

The utmost compound $NdFe_3(BO_3)_4$ has the noncentrosymmetric space group (SG) *R32* below room temperature,

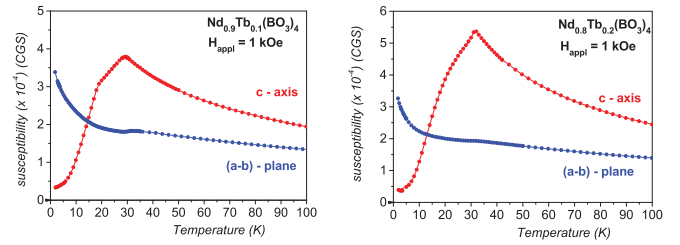FIG. 2. Temperature dependence of dc-magnetic susceptibilities along the *c* axis and in the *ab* plane in $Nd_{0.9}Tb_{0.1}Fe_3(BO_3)_4$ and $Nd_{0.8}Tb_{0.2}Fe_3(BO_3)_4$.

while $TbFe_3(BO_3)_4$ undertakes a structural phase transition at about 240 K from the *R32* to the less symmetric *P3₁21* [17]. Single crystal neutron diffraction of the substituted ferroborates $Nd_{1-x}Tb_xFe_3(BO_3)_4$ does not give an unambiguous answer to which SG is realized: *R32* or *P3₁21*. However, our magnetoelectric measurements (not shown in this work) do not suggest any structural phase transition in the temperature range of 2–300 K, and therefore, the space group *R32*, as in $NdFe_3(BO_3)_4$ is assumed.

In this SG three Fe atoms occupy the 9d Wyckoff site with coordinates: Fe1 (0, x, 0), Fe2 ($-x$, $-x$, 0), and Fe3 (x, 0, 0) (in the hexagonal setting), while the rare earth atoms occupy the 3a site with coordinate (0, 0, 0). The other atomic positions in a chemical cell multiply by the trigonal translations: (0, 0, 0), (2/3, 1/3, 1/3), and (1/3, 2/3, 2/3). Refinement of the nuclear reflections at 2 K gives $x = 0.5504(2)$ and $x = 0.5508(2)$ for $Nd_{0.9}Tb_{0.1}Fe_3(BO_3)_4$ and $Nd_{0.8}Tb_{0.2}Fe_3(BO_3)_4$, respectively.

B. Magnetic structure

Magnetic susceptibility measurements clearly demonstrate that magnetic order appears below $\sim$30–31 K (Fig. 2). The anisotropy in the magnetic susceptibility in the magnetic field applied within the *ab* plane and along the *c* axis indicates that the magnetic structure at low temperature should be close to the *"easy-axis"* type, where the moments are near the *c* axis, and therefore, the magnetic structure is closer to that of $TbFe_3(BO_3)_4$.

In addition to the maximum in the temperature dependence of the magnetic susceptibility along the *c* axis, which is associated with an antiferromagnetic ordering at the Néel point, one could also note a change in the susceptibility slope at about $\sim$15–18 K. This feature is also observed in the temperature dependence of the (3 3 3/2) magnetic reflection [see Fig. 3(a)].

The profiles of the magnetic reflection (3 3 3/2) and (0 0 3/2) measured at different temperatures [see Figs. 3(c) and 3(d)] do not demonstrate the appearance of any marked features, for example peak shape distortion, which could shed light on the origin of this "kink."

In magnetic diffraction, the only moment projection, which is perpendicular to the diffraction vector, is measured. So, the intensity of the reflection (0 0 3/2) is proportional to the square of the resulting moment projection in the basal plane. From Fig. 3(d) it is seen that this component exists at all temperatures and increases with temperature increase.
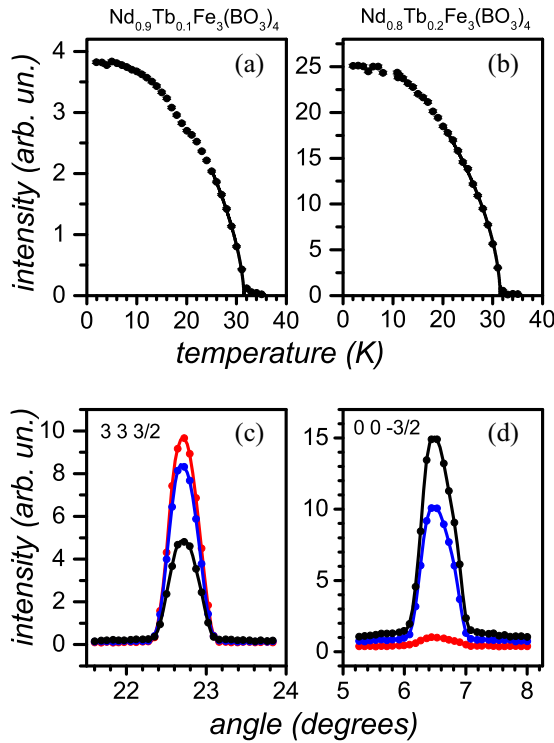
FIG. 3. Temperature dependencies of the intensity of the magnetic reflection (3 3 3/2) for $Nd_{0.9}Tb_{0.1}Fe_3(BO_3)_4$ (a) and $Nd_{0.8}Tb_{0.2}Fe_3(BO_3)_4$ (b). The solid lines are fits to a power law. Profiles of the magnetic reflection (3 3 3/2) (c) and (0 0 −3/2) (d) for $Nd_{0.9}Tb_{0.1}Fe_3(BO_3)_4$ at 2 K (in red), 15 K (in blue), and 25 K (in black).

It means that the "easy-axis," magnetic structure sustains and the observed "kink" probably originates from rearrangement (reorientation) of the spins in the basal plane.

Unfortunately the multidomain structure in the plane (which will be discussed below), does not allow us to resolve this spin rearrangement in the neutron diffraction experiment. The fitting of the temperature dependency of the integral peak intensity of the reflection (3 3 3/2) (Fig. 3) near the magnetic transition by a power law indicates the Néel temperature of 31.4(2) K for both compositions.

Below the magnetic transition, magnetic reflections with $l = (2n + 1)/2$ indexes are observed. These reflections can be indexed with propagation vector **k** = [0 0 3/2] in a hexagonal unit cell (SG *R32*) as accepted for $NdFe_3(BO_3)_4$ or with **k** = [0 0 1/2] in a primitive rhombic unit cell (SG $P3_121$) as accepted in $TbFe_3(BO_3)_4$ [10]. Since in our case the SG *R32* has been assumed, the propagation vector **k** = [0 0 3/2] was used in the refinement. In contrast with $NdFe_3(BO_3)_4$, no incommensurate magnetic structure was detected within the limits of the experimental resolution [Figs. 3(c) and 3(d)].

The magnetic cell of the substituted ferroborates $Nd(Tb)Fe_3(BO_3)_4$ is twice the chemical cell and comprises 24 magnetic atoms. There are four independent magnetic sublattices in the chemical cell: three of Fe atoms and one of a rare earth sublattice. The trigonal translations form the planes with alternate magnetic moments, which are shifted along the direction [−1 1 0] at the translation of 1/3 along the *c* axis.
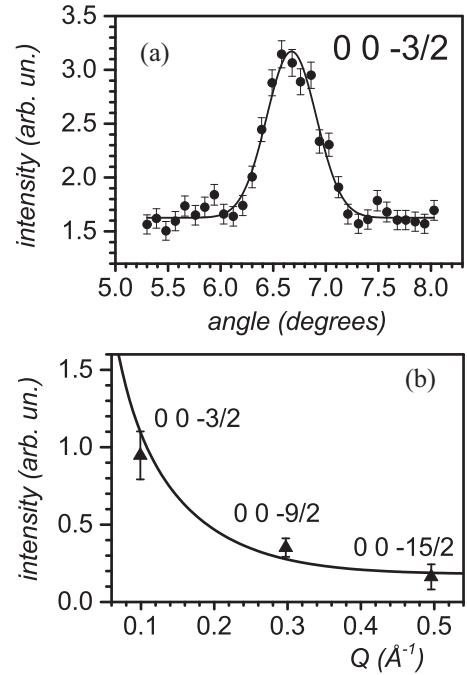

FIG. 4. (a) Profile of the reflection (0 0 −3/2), measured at 2 K for $Nd_{0.8}Tb_{0.2}Fe_3(BO_3)_4$. (b) The Q dependence of the intensities of the (0 0 *l*) reflections. The solid line is a calculated curve (see text).

As it was marked above, in magnetic diffraction, the only moment projection, which is perpendicular to the diffraction vector, is measuring. In our experiments, we observed the magnetic reflections (0 0 −3/2), (0 0 −9/2), and (0 0 −15/2) that confirms the existence of the in-plane components of the magnetic moments (Fig. 4).

The observed (0 0 *l*) reflections are weak, less than 2% of the strongest magnetic reflection. To be sure that they are not due to multiple scattering, the Q dependence of their intensities was calculated [Fig. 4(b)]. In this calculation, the contribution of the additional, independent on Q, scattering to the total intensity of the reflections was estimated to be less than 9%, which confirms their magnetic nature. Most probably this contribution resulted from the multiple scattering.

It is known that the moments of Nd^{3+} and the moments of Tb^{3+} are antiparallel [7,8,10]. It means that their average contribution to the reflection intensity is small in comparison with the Fe spin. Therefore, the form factor of the Fe^{3+} ion [18] was used in the above calculations.

IV. SYMMETRY ANALYSIS OF THE MAGNETIC STRUCTURES

The expected magnetic structures have been analyzed within the symmetry approach [4,19,20]. The crystal structure of the $ReFe_3(BO_3)_4$ could be represented by a set of shifted identical horizontal layers spaced one third of a period along the *c* axis. Atoms in the different layers are connected by the trigonal translations.

For a description of the magnetic structure, we consider six Fe spins: M_1–M_6. The first three, M_1, M_2, and M_3, belong to one horizontal layer (parallel to the basal plane), and the other three, M_4, M_5, and M_6, lie in the adjacent parallel layer at

TABLE I. Irreducible representations of the reduced $\tilde{G}32$ group and the transformational properties of the basis vectors of the Fe sublattice, **M**, **L**, $\mathbf{B_1}$, $\mathbf{B_2}$, $\tilde{\mathbf{B}}_1$, $\tilde{\mathbf{B}}_2$, and R sublattice (**m**, **l**) (from Refs. [4,20]).

Irreps	E	T_1	C_3	2_x	**M, m**	**L, l**	$\mathbf{B_1}, \mathbf{B_2}, \tilde{B}_1, \tilde{B}_2$
Γ_1	1	1	1	1			$\tilde{B}_{1y}\text{-}\tilde{B}_{2x}$
$\Gamma_1{'}$, (mT1)	1	-1	1	1			$B_{1y}\text{-}B_{2x}$
Γ_2	1	1	1	-1	M_z, m_z		$\tilde{B}_{1x}+\tilde{B}_{2y}$
$\Gamma_2{'}$, (mT2)	1	-1	1	-1		L_z, l_z	$B_{1x}+B_{2y}$
Γ_3	1	1	$R^{*)}$	$\begin{pmatrix}1 & 0\\0 & -1\end{pmatrix}$	$\begin{pmatrix}M_x\\M_y\end{pmatrix}$, $\begin{pmatrix}m_x\\m_y\end{pmatrix}$		$\begin{pmatrix}\tilde{B}_{1y}+\tilde{B}_{2x}\\\tilde{B}_{1x}-\tilde{B}_{2y}\end{pmatrix}$, $\begin{pmatrix}\tilde{B}_{1z}\\\tilde{B}_{2z}\end{pmatrix}$
$\Gamma_3{'}$, (mT3)	1	-1	R	$\begin{pmatrix}1 & 0\\0 & -1\end{pmatrix}$		$\begin{pmatrix}L_x\\L_y\end{pmatrix}$, $\begin{pmatrix}l_x\\l_y\end{pmatrix}$	$\begin{pmatrix}B_{1y}+B_{2x}\\B_{1x}-B_{2y}\end{pmatrix}$, $\begin{pmatrix}B_{1z}\\B_{2z}\end{pmatrix}$

$^{*}R$ is the matrix of the rotation on $120°$.

a distance of $c/3$. Vectors $\mathbf{m}_1$ and $\mathbf{m}_2$ denote the rare earth moments.

In the used approach the so-called reduced space group $\tilde{G}32$ with a magnetic cell which is twice of a chemical cell was used. In this group, in addition to the generators of the initial group *R32*: E—the unit transformation, C_3—the third-order axis along the *c* axis, and 2_x—the second-order axis, lying in the basal plane along the *a* axis, an additional symmetry element T_1, the translation along the *c* axis, was used [4]. According to the Landau theory, in describing the magnetic phase transition it is more convenient instead of the individual spins M_1–M_6 to use the symmetrized combinations corresponding to the irreducible representations of the $\tilde{G}32$ group (see Table I).

$$\mathbf{M} = \frac{1}{6}(\mathbf{M}_1 + \mathbf{M}_2 + \mathbf{M}_3 + \mathbf{M}_4 + \mathbf{M}_5 + \mathbf{M}_6),$$

$$\mathbf{L} = \frac{1}{6}(\mathbf{M}_1 + \mathbf{M}_2 + \mathbf{M}_3 - \mathbf{M}_4 - \mathbf{M}_5 - \mathbf{M}_6),$$

$$\mathbf{B}_1 = \frac{\sqrt{3}}{6}(\mathbf{M}_1 - \mathbf{M}_2 - \mathbf{M}_4 + \mathbf{M}_5),$$

$$\mathbf{B}_2 = \frac{1}{6}(\mathbf{M}_1 + \mathbf{M}_2 - 2\mathbf{M}_3 - \mathbf{M}_4 - \mathbf{M}_5 + 2\mathbf{M}_6)$$

$$\tilde{\mathbf{B}}_1 = \frac{\sqrt{3}}{6}(\mathbf{M}_1 - \mathbf{M}_2 + \mathbf{M}_4 - \mathbf{M}_5),$$

$$\tilde{\mathbf{B}}_2 = \frac{1}{6}(\mathbf{M}_1 + \mathbf{M}_2 - 2\mathbf{M}_3 + \mathbf{M}_4 + \mathbf{M}_5 - 2\mathbf{M}_6),$$

$$\mathbf{m} = \frac{1}{2}(\mathbf{m}_1 + \mathbf{m}_2),$$

$$\mathbf{l} = \frac{1}{2}(\mathbf{m}_1 - \mathbf{m}_2). \tag{1}$$

The distortion of the collinear structure, given by the vector **L**, is defined by a pair of the vectors $\mathbf{B}_1$, $\mathbf{B}_2$ and results in a complex antiferromagnetic structure, which is described by the thermodynamic potential [4]:

$$\Phi = \tfrac{1}{2}\Lambda_1 \mathbf{L}^2 + \tfrac{1}{2}\Lambda_2\big(\mathbf{B}_1^2 + \mathbf{B}_2^2\big) + \alpha_1[L_x(B_{1y} + B_{2x})$$
$$+ L_y(B_{1x} - B_{2y})] + \alpha_2 L_z(B_{1x} + B_{2y}) + ..., \tag{2}$$

where $\Lambda_{1,2}$ and $\alpha_{1,2}$ are phenomenological constants determined by isotropic and anisotropic Fe-Fe interactions,

respectively. The latter terms are responsible for the "fine" magnetic structure. There are also other anisotropic contributions in Eq. (2) controlling the spin orientation with respect to crystallographic axes, which are omitted here for the sake of simplicity.

The "unprimed" irreducible representations in Table I correspond to the so-called first kind "black-white" groups [21,22]. For them the spin reversal operator is not associated with translations. The magnetic unit cell is the same as the crystallographic cell.

The "primed" groups correspond to the second kind "black-white" groups. They have the translations associated with spin reversal, so that the "magnetic primitive cell" is bigger than the crystal primitive cell, and they are the object of our attention.

Each irreducible representation corresponds to a particular magnetic configuration and is described as a superposition of the basis functions shown in Table I. For example, the magnetic order of the *"easy-axis"* type with the spins oriented along the *c* axis is described by one-dimensional representation $\Gamma_2{'}$. The magnetic order of the *"easy-plane"* type with the spins within the *ab* plane is described by two-dimensional representation $\Gamma_3{'}$. In this case, the spins could be aligned along the axis of the second order or aligned perpendicular to it. Furthermore, an intermediate (canted) phase is possible.

The vector **L** describes a collinear antiferromagnetic ordering in two ferromagnetic Fe layers spaced by $c/3$, with alternate moments in the adjacent layers. This is the main type of the magnetic order in the ferroborates.

As already noticed, neutron diffraction unambiguously shows the existence of the *z* component of the magnetic moments, i.e., $L_z \neq 0$ and $l_z \neq 0$. Therefore, we will consider the following configurations only.

(1) *"Easy-axis"* magnetic configuration, which corresponds to the one-dimensional irreducible representation $\Gamma_2{'}$.

(2) *"Easy-plane"* magnetic configurations, which correspond to the two-dimensional irreducible representation $\Gamma_3{'}$. In the frame of this representation several structures are possible, namely:

(a) Configuration of the moments lying along the second order axis.

(b) Configuration of the moments lying perpendicular to the second order axis.
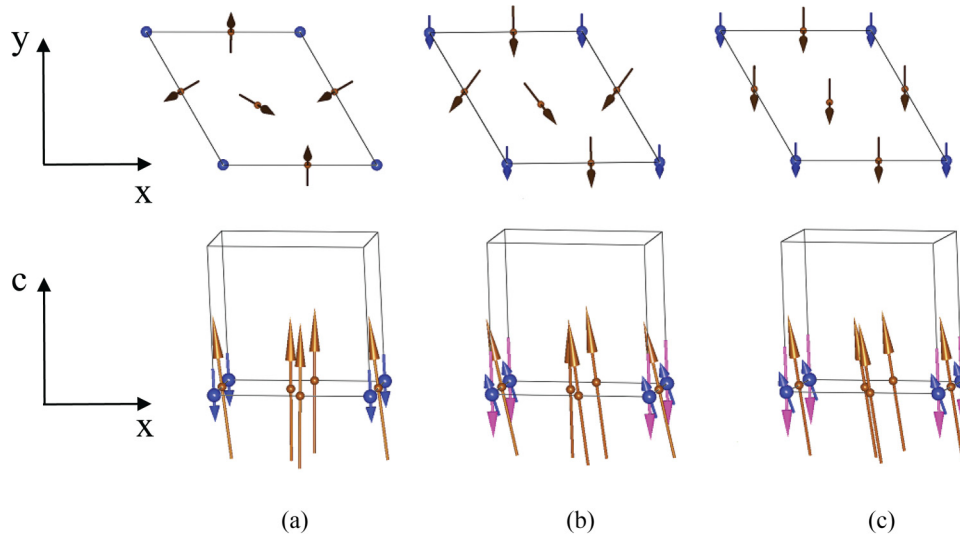
FIG. 5. Models of magnetic structures (configurations) allowed by symmetry. Yellow, blue, and magenta arrows correspond to Fe, Nd, and Tb ions. (a) *"Easy-axis"* structure, the Nd and Tb moments are aligned along the *c* axis and are indistinguishable. They are shown by one arrow. (b) *"Angular"* structure with the vector **L** lying within the *yz* plane (in the orthogonal system). (c) *Collinear* structure. In all models Tb moments are Ising type and they are aligned along the *c* axis. The projections of the magnetic moments on the basis plane are shown enlarged. Only Fe atoms in the basal plane are shown. The *x* axis in the orthogonal system coincides with the *a* axis in the hexagonal system.

(c) Configuration of the moments lying within a basal plane at an arbitrary angle to the second order axis.

(3) *"Angular"* configuration, driven by the representation Γ_{23}', which includes the considered above representations Γ_2' and Γ_3'.

The term *"angular structure"* means that the main order parameter, antiferromagnetic vector **L**, does not align along a certain crystallographic axis but has non-zero components, which value are changing continuously with a temperature or magnetic field [23].

The *"easy-axis,"* the *"angular,"* and the simple collinear magnetic structures are shown in Fig. 5. The main difference between the considered models is the orientation of the main antiferromagnetic vector **L** [Eq. (1)]. In the "easy-axis" structure the vector **L** is directed exactly along the *c* axis, while in the "angular" structure the vector **L** tilts from this axis but is lying within the *yz* plane. The collinear structure is the simplified option of the "easy-axis" and the "angular" structures, when vectors $\mathbf{B_1} = \mathbf{B_2} = 0$. The components of the magnetic moment, coupled by the symmetry constraints, are shown in the Supplemental Material [15]. The results of the above symmetry analysis are consistent with the analysis reported for $NdFe_3(BO_3)_4$ [7] and $CeFe_3(BO_3)_4$ [6], which used the standard approach realized by the codes BasIreps (Fullprof Suite) [16] and SARAh software [24], respectively.

The considered above magnetic configurations are fully consistent with the configurations, which one could derive using the programs k-SUBGROUPSMAG and MAGMOD-ELIZE from the Bilbao Crystallographic Server [25] for the paramagnetic group *R32* and the propagation vector **k** = [0 0 3/2].

For example, one can show that the "easy-axis" magnetic configuration corresponds to the nonpolar Shubnikov magnetic group R_I32 (number BNS [26] 155.48). The corresponding designations of the "primed" irreducible representation

are shown in the brackets in Table I. It should note that our approach focuses not on the arrangement of the individual magnetic moments but on the symmetrized functions of the moments [Eq. (1)], which are responsible for the corresponding terms in the free energy deconvolution [Eq. (2)].

V. NEUTRON DIFFRACTION EXPERIMENT: REFINEMENT OF THE MAGNETIC STRUCTURES AND ITS FEATURES

A. Orientation of the magnetic moments within the basal plane

Symmetry analysis allows the existence of three equivalent domains corresponding to three crystallographic axes in the *ab* plane (Fig. 6). Indeed, the refinement of neutron diffraction data for all configurations turns out to be possible only if one assumes the existence of these domains.

Within the *"angular"* model the mutual orientation of the Fe spins in the basal plane is determined by the symmetry (see Supplemental Material). For example, if the vector **L** lies in the *yz* plane, the spin configuration of the Fe ions is described by the five variable parameters $M_1 = M_2$, M_3, $\Theta_1 = \Theta_2$, Θ_3, and ϕ. The latter define the in-plane orientation of the vectors $\mathbf{M}_1$ and $\mathbf{M}_2$, at that $\mathbf{M}_{1x} = -\mathbf{M}_{2x}$ and $\mathbf{M}_{1y} = \mathbf{M}_{2y}$. Moment
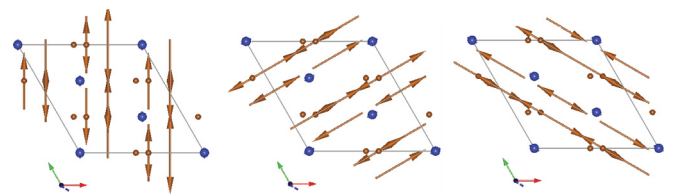

FIG. 6. Projections of the magnetic configurations on the basal plane in three domains, assuming a collinear structure as an example.

M_3 is aligned perpendicular to the x axis, so the corresponding ϕ_3 is either 270 or 90 degrees.

In the cases of the *"easy-axis"* and collinear models the χ^2 residual does not show any appreciable minimum on varying the orientation of the Fe spins within the ab plane. Therefore, the corresponding angles were fixed at 270 or 90 degrees. The indeterminacy of the direction of the Fe spin in the basal plane in the collinear phase has been reported for NdFe$_3$(BO$_3$)$_4$ [8] and CeFe$_3$(BO$_3$)$_4$ [6]. We suppose that such a situation is caused by very small anisotropy within the basal plane. It results in multidomain structure when all orientations of the spin in the basal plane are equally probable. The three domains approach should be considered as an adequate model only.

B. Constraints implied in the refinement

As it has been noted above, the magnetic moments on the Nd and Tb sites, induced by the exchange field from the Fe sublattice, are directed in opposite, that is explained by the different Landé factors of the rare-earth ions. Indeed, since the exchange field on the rare earth sites is proportional to $(g_{Nd(Tb)} - 1)/g_{Nd(Tb)}$ and $g_{Nd} - 1 = 8/11 - 1 < 0$, while $g_{Tb} - 1 = 3/2 - 1 > 0$, the magnetic moments of Nd^{3+} and Tb^{3+} are antiparallel, which results in a small net moment on the rare earth site.

The small contribution of the rare earth magnetic moment to the intensity of the magnetic reflections, compared with the contribution from the Fe spin, leads to the fact that the magnitude and the orientation of the rare earth moments cannot be refined reliably. Moreover, the large number of variables and a "shallow" minimum in the χ^2 residual leads to multiple "false" solutions, which are practically impossible to resolve. Therefore, to get the physically meaningful solution we used simple constraints, implied by the fact that the magnetic order in the rare earth sublattice is induced by the Fe sublattice.

Additional constraints connecting the variables can be written based on a simple model, using the following parameters of the ground Kramers doublet of Nd^{3+} and quasi-doublet of Tb^{3+}, known from the literature for *"easy-plane"* and *"easy-axis"* compounds NdFe$_3$(BO$_3$)$_4$ and TbFe$_3$(BO$_3$)$_4$, respectively.

(i) The magnetic moments along and perpendicular to the c axis for NdFe$_3$(BO$_3$)$_4$ were estimated from the optical spectroscopy and magnetic resonance measurements: $\mu_c^{Nd} = 0.65\ \mu_B$ and $\mu_{ab}^{Nd} = 1.2\ \mu_B$, respectively [27,30].

(ii) The exchange splitting of the Nd^{3+} ground doublet at low temperatures, when the Fe sublattice is "saturated," in the "easy axis" state $\Delta_c^{Nd} = 9.13$ cm^{-1}, and the "easy-plane" state $\Delta_{ab}^{Nd} = 8.7$ cm^{-1}, taken from AFMR data [28–30].

(iii) Since the Tb^{3+} ion is an Ising moment, aligned along the c axis, we'll use the moment projections known for TbFe$_3$(BO$_3$)$_4$: $\mu_c^{Tb} = 8.6\ \mu_B$ [10], $\mu_{ab}^{Tb} = 0$, and the exchange splitting in the uniaxial state of the Fe subsystem $\Delta_c^{Tb} = 30$ cm^{-1}(Ref. [31]).

Unlike the utmost *"easy-plane"* NdFe$_3$(BO$_3$)$_4$ and *"easy-axis"* TbFe$_3$(BO$_3$)$_4$ compounds, in the substituted compositions the Fe spin and, consequently, the exchange magnetic field is tilted from the c axis. Therefore, the projections of the rare earth magnetic moments are proportional to the projections of the exchange field: $L_0 \sin\theta_{Fe}$ and $L_0 \cos\theta_{Fe}$.
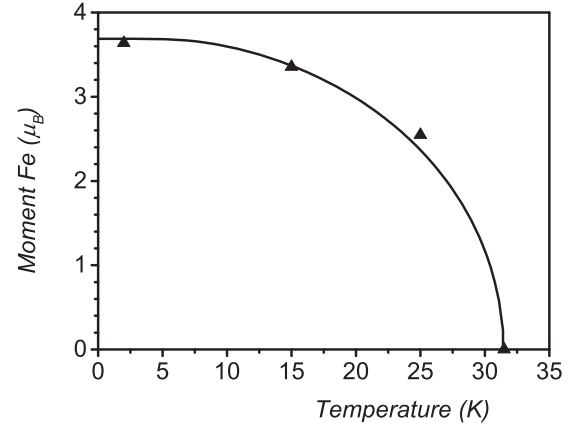

FIG. 7. Refined Fe^{3+} spin (triangles) at different temperatures and its mean-field approximation (solid line).

Here, L_0 is the normalized Fe^{3+} spin. Its temperature dependence could be calculated according to the mean-field approximation of the measured temperature dependence of Fe^{3+} spin and is given as a solid line in Fig. 7. The angle θ_{Fe} determines the orientation of L_0 relative to the c axis.

In first approximation, the intrinsic rare earth magnetic moments can be expressed through the moments μ_{ab}^{Nd}, μ_c^{Nd}, μ_c^{Tb} and the exchange splitting Δ_{ab}^{Nd}, Δ_c^{Nd}, and Δ^{Tb}, known for the utmost compounds NdFe$_3$(BO$_3$)$_4$ and TbFe$_3$(BO$_3$)$_4$. Then, the magnetic moments of the Nd^{3+} and Tb^{3+} in substituted compounds can be written as [20]:

$$
\vec{m}^{Nd} = \begin{pmatrix} m_{ab}^{Nd} \\ m_c^{Nd} \end{pmatrix}
$$

$$
\equiv \begin{pmatrix} L_0 \sin\theta_{Fe}\mu_{ab}^{Nd}\Delta_{ab}^{Nd}/\Delta^{Nd} \\ L_0 \cos\theta_{Fe}\mu_c^{Nd}\Delta_c^{Nd}/\Delta^{Nd} \end{pmatrix} \cdot \tanh(\Delta^{Nd}/2k_B T)
$$

$$
m^{Tb} = m_c^{Tb} \equiv \mu_c^{Tb}\tanh(\Delta^{Tb}/2k_B T). \tag{3}
$$

The resulting exchange splitting of Nd^{3+} and Tb^{3+} ground states in the magnetic field of the Fe subsystem, for the substituted compositions, can be written as:

$$
\Delta^{Nd} = \left[\left(\Delta_c^{Nd}L_0\cos\theta_{Fe}\right)^2 + \left(\Delta_{ab}^{Nd}L_0\sin\theta_{Fe}\right)^2\right]^{1/2},
$$

$$
\Delta^{Tb} = \Delta_c^{Tb}L_0\cos\theta_{Fe}. \tag{4}
$$

The magnitude of the Nd^{3+} magnetic moment and its orientation can be written as:

$$
m^{Nd} = \frac{\sqrt{\left(\mu_{ab}^{Nd}\Delta_{ab}^{Nd}L_0\sin\theta_{Fe}\right)^2 + \left(\mu_c^{Nd}\Delta_c^{Nd}L_0\cos\theta_{Fe}\right)^2}}{\Delta^{Nd}}
$$

$$
\times tanh(\Delta^{Nd}/2k_B T) \tag{5}
$$

$$
\cos\theta_{Nd} = \frac{\mu_c^{Nd}\Delta_c^{Nd}\cos\theta_{Fe}}{\sqrt{\left(\mu_{ab}^{Nd}\Delta_{ab}^{Nd}\sin\theta_{Fe}\right)^2 + \left(\mu_c^{Nd}\Delta_c^{Nd}\cos\theta_{Fe}\right)^2}}. \tag{6}
$$

The values μ_c^{Nd}, μ_{ab}^{Nd}, Δ_c^{Nd}, and Δ_{ab}^{Nd} we consider as fixed parameters. The magnitude of the Fe^{3+} spin, its deviation from the c axis θ_{Fe}, as well as the deviation of the Nd^{3+}
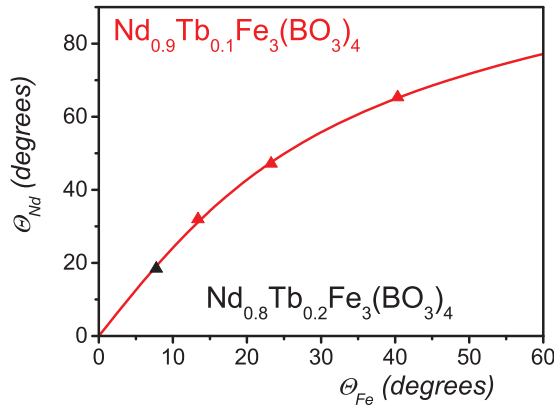
FIG. 8. Red line is the calculated dependence of the inclination angle Θ_{Nd} of the Nd^{3+} moment versus the angle Θ_{Fe} of the Fe^{3+} spin. Red triangles are the results of the refinement under the constraints for temperature points 2 K, 15 K, and 25 K for $Nd_{0.9}Tb_{0.1}Fe_3(BO_3)_4$. Black triangle corresponds to $Nd_{0.8}Tb_{0.2}Fe_3(BO_3)_4$ at 2 K. The calculation for 2 K is performed in the frame of the *"angular"* model; for 15 K and 25 K the calculation is performed for the collinear model. Note that in $NdFe_3(BO_3)_4$ $\Theta_{Nd} = \Theta_{Fe} = 90°$, while in $TbFe_3(BO_3)_4$ $\Theta_{Nd} = \Theta_{Fe} = 0°$.

moment from the c axis θ_{Nd} are variables. They are constrained by Eqs. (5) and (6).

While the in-plane projection μ_{ab}^{Nd} of the magnetic moment Nd^{3+} is known from neutron scattering experiments for the *"easy-plane"* compound $NdF_3(BO_3)_4$, the projection μ_c^{Nd} along the c axis is known only approximately from the magnetic susceptibility calculation [27]. In order to describe self-consistently the temperature dependence μ^{Nd} and to also satisfy the reasonable value of μ^{Tb}, we used the fixed parameter $\mu_c^{Nd} = 0.45\ \mu_B$.

The straightforward calculation using the formula (6), and also taking into account the above parameters, gives the relation between the deviation angles $\Theta_{Nd}(\Theta_{Fe})$ shown in Fig. 8. This dependence is not influenced by the temperature in the
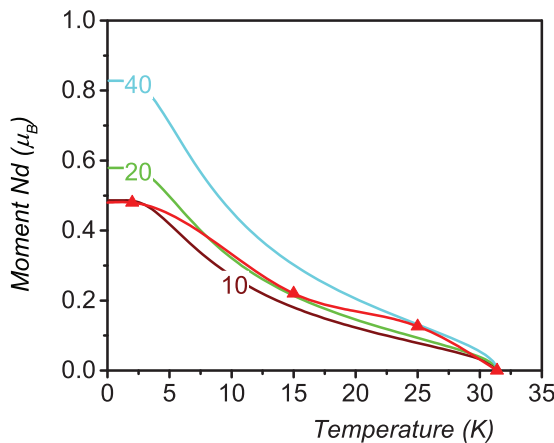

FIG. 9. The calculated temperature dependencies of Nd^{3+} moment (solid lines) for fixed angles Θ_{Fe}: 10, 20, and 40 degrees. The red triangles show Nd^{3+} moments corresponding to the angles Θ_{Fe}: 11.9(2), 23.2(1), and 40.4(2) degrees, refined for $Nd_{0.9}Tb_{0.1}Fe_3(BO_3)_4$ at 2 K, 15 K, and 25 K. Red line is a guide for the eye.
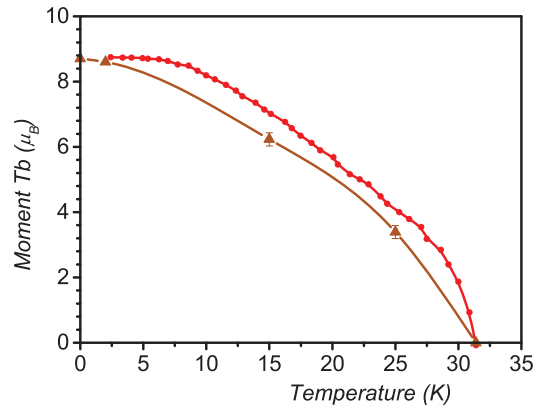

FIG. 10. Temperature dependence of the Tb^{3+} moment (brown triangles) for $Nd_{0.9}Tb_{0.1}Fe_3(BO_3)_4$. Brown line is a guide for the eye. Red points correspond to the temperature dependence for $TbFe_3(BO_3)_4$ [10].

approximation used, in which the van Vleck' contribution to susceptibility is negligible. The "fine structure" of the Fe subsystem associated with vectors $\mathbf{B}_1$ and $\mathbf{B}_2$ is also neglected.

C. Refinement, the models found in the experiment, magnitudes and directions of the magnetic moments

Since the averaged rare earth moment is small in comparison with the Fe spin, the contribution of the latter to the intensity of the magnetic reflections dominates. As a result, the self-consistent refinement is only weakly dependent on the magnitude and orientation of the rare earth moment.

This gives grounds to use the same $\Theta_{Nd}(\Theta_{Fe})$ dependence and the task parameters for all possible models. Using this constraint, we performed the refinement of the neutron diffraction data for the general model with independently refined magnitudes and directions of all Fe spins. As well we explored the *"easy-axis"* and the collinear models with equal magnitudes of the Fe spins in three equivalent crystallographic positions.
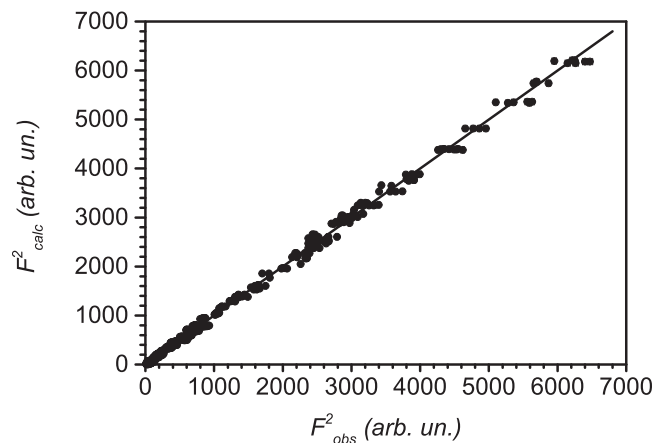

FIG. 11. The results of refinement of the *"angular"* magnetic configuration, with the vector $\mathbf{L}$ within the yz plane found at 2 K for $Nd_{0.9}Tb_{0.1}Fe_3(BO_3)_4$. $R_{F^2} = 5.75$, $R_{F^2w} = 8.40$, $R_F = 4.80$, and there are 717 reflections in the refinement. Errors do not exceed the symbol size.

TABLE II. Goodness-of-fit parameters for different models at 2 K.

	χ^2	R_{F^2}	R_{F^2w}	R_F
	$Nd_{0.9}Tb_{0.1}Fe_3(BO_3)_4$			
"angular"	58.8	5.75	8.40	4.80
collinear	80.0	6.59	9.86	5.64
"easy-axis"	110.0	7.76	11.5	7.12
	$Nd_{0.8}Tb_{0.2}Fe_3(BO_3)_4$			
"angular"	76.7	6.37	8.37	5.59
collinear	90.6	6.99	9.11	6.38
"easy-axis"	110.0	7.39	10.0	7.30

In Fig. 8 the refined deviations Θ_{Fe} and Θ_{Nd} for Fe^{3+} and Nd^{3+} moments, respectively, using the rigid coupling $\Theta_{Nd}(\Theta_{Fe})$, are shown for 2 K, 15 K, and 25 K. For any angle Θ_{Fe} the corresponding dependence of the Nd^{3+} moment on temperature $m^{Nd}(T)$ can be calculated using Eq. (5). In Fig. 9 the temperature dependencies of $m^{Nd}(T)$ calculated for the fixed angles Θ_{Fe}: 10, 20, and 40 degrees are shown as examples. Thus, using the refined Θ_{Fe} one can define the corresponding Nd^{3+} moments at every temperature point. Note that the magnetic moment of Nd^{3+} in the substituted compound $Nd_{0.9}Tb_{0.1}Fe_3(BO_3)_4$ is smaller than 1.2 μ_B in pure $NdFe_3(BO_3)_4$, evaluated from the neutron diffraction [8], that is explained by the inclination from a plane the exchange magnetic field induced by Fe^{3+}.

Because of the strong correlation between Tb^{3+} and Nd^{3+} moments, which occupy the same crystallographic positions, their simultaneous refinement is impossible. Therefore to separate magnetic contributions of different rare earth ions we used the circumstance that the Tb moment is an Ising moment and is aligned along the *c* axis. So its direction could be fixed and the only moment value is varying.

Fixing the obtained value of the Nd^{3+} moment (shown by the red triangles in Fig. 9), the refined Tb^{3+} moment is shown in Fig. 10. For comparison, the temperature dependence for $TbFe_3(BO_3)_4$ from the powder neutron diffraction [10] is shown as well.

It should be noted that the temperature dependence of the Tb^{3+} moment in the substituted compound markedly differs from the temperature dependence for $TbFe_3(BO_3)_4$ [10]. This feature is caused by the variation of the Fe^{3+} spin direction with temperature in the substituted compounds.

For $Nd_{0.8}Tb_{0.2}Fe_3(BO_3)_4$, with the larger concentration of Tb, the measurements were carried out only at 2 K. The similar self-consistent refinement, performed under the same conditions, with the same dependence $\Theta_{Nd}(\Theta_{Fe})$, gives smaller angles Θ_{Fe} and Θ_{Nd} marked by the black triangle in Fig. 8. It is an expected result, because the $Nd_{0.8}Tb_{0.2}Fe_3(BO_3)_4$ is close to the *"easy-axis"* compound $TbFe_3(BO_3)_4$.

The independent refinement gives the Tb^{3+} moment a little bit more than the free ion moment. It turns out that a value close to the expected moment of 8.6 μ_B can be obtained assuming that the real Tb concentration is 21.8% instead of the nominal 20%.

For both compositions $Nd_{0.9}Tb_{0.1}Fe_3(BO_3)_4$ and $Nd_{0.8}Tb_{0.2}Fe_3(BO_3)_4$, at 2 K, the refinement evidences in favor of the *"angular"* configuration with the vector **L**, lying within the *yz* plane (see Table II). The expected *"easy-axis"* model shows worse goodness-of-fit parameters, bringing us to the preservation of the *"angular"* configuration. As an example, the results of the refinement of the *"angular"* magnetic configuration in $Nd_{0.9}Tb_{0.1}Fe_3(BO_3)_4$ at 2 K is shown in Fig. 11.

At 15 K the refinement in the frame of the general model, with the independent magnitudes and the directions of Fe spins, reveals the *"angular"* configuration, which is very close to the collinear model. The Fe spins are aligned along the mean direction ϕ_{Fe} of 81(7) degrees and Θ_{Fe} of 23(1) degrees. The "goodness-of-fit" parameters of these two models are very close, so these models are unresolved.

At 25 K, the refinement definitely evidences in favor of the collinear model. Results of the refinement for the possible magnetic structures are shown in Table III.

TABLE III. Results of the refinement for $Nd_{0.9}Tb_{0.1}Fe_3(BO_3)_4$ and $Nd_{0.8}Tb_{0.2}Fe_3(BO_3)_4$. R factors (goodness-of-fit parameters), values of the magnetic moments, and their directions.

	T, K	R_{F^2}, R_{F^2w}, R_F	M_{Fe}, μ_B*	m^{Nd}, μ_B, fixed	θ_{Nd}, degrees	θ_{Fe}, degrees*	ϕ_{Fe}, degrees*
		$Nd_{0.9}Tb_{0.1}Fe_3(BO_3)_4$					
"angular," yz model	2	5.75, 8.40, 4.80	3.47(1), 3.98(2)	0.48	31.9(5)	13.7(2), 12.7(3)	238(1), 302(1), 270
"angular," general model	15	6.21, 8.68, 5.10	3.10(4), 3.38(8), 3.58(8)	0.22	56(2)	30(2), 21(2), 20.3(6)	−111(9), −90(9), −101(9)
collinear	15	6.57, 9.90, 5.80	3.38(1)	0.22	47.2(3)	23.3(6)	undefined
collinear	25	7.42, 10.3 6.48	2.54(1)	0.13	65.3(2)	40.3(3)	undefined
		$Nd_{0.8}Tb_{0.2}Fe_3(BO_3)_4$					
"angular," yz model	2	6.75, 8.66, 5.74	4.04(3), 3.74(7)	0.48	18.4(5)	8.08(2), 7.2(3)	−172(2), −8(2), 270

*In the *"angular"* models Fe spins M_{Fe} and their deviations Θ_{Fe} in three crystallographic positions of Fe1 (0, *x*, 0), Fe2 (−*x*, −*x*, 0), and Fe3 (*x*, 0, 0) are nonequivalent. Therefore, all corresponding values are shown.

TABLE IV. Results of refinement expressed in the terms of vectors **L**, **B**$_1$, and **B**$_2$.

	L	θ_L	ϕ_L	B$_{1x}$, B$_{1y}$, B$_{1z}$	B$_{2x}$, B$_{2y}$, B$_{2z}$
Nd$_{0.9}$Tb$_{0.1}$Fe$_3$(BO$_3$)$_4$ 2 K (*"angular"*)	3.62(2)	12.2(1)	90(1)	$-0.513(6)$; 0.00(2); 0.000(1)	0.00(1); 0.127(2); $-0.34(1)$
Nd$_{0.9}$Tb$_{0.1}$Fe$_3$(BO$_3$)$_4$ 15 K (*"angular"*)	3.34(1)	24.3(6)	81(7)	$-0.309(3)$, $-0.0(1)$, 0.23(6)	$-0.2(2)$, $-0.08(5)$, $-0.30(3)$
Nd$_{0.9}$Tb$_{0.1}$Fe$_3$(BO$_3$)$_4$ 15 K (*collinear*)	3.38(1)	23.3(1)	90	0	0
Nd$_{0.9}$Tb$_{0.1}$Fe$_3$(BO$_3$)$_4$ 25 K (*collinear*)	2.55(1)	40.3(1)	90	0	0
Nd$_{0.8}$Tb$_{0.2}$Fe$_3$(BO$_3$)$_4$ 2 K (*"angular"*)	3.91(4)	3.1(1)	90(1)	$-0.65(1)$; 0.0(2); 0.000(1)	0.000(1); 0.26(1); 0.19(2)

VI. DISCUSSION

A weak deviation of the magnetic moments from the c axis was previously detected in TbFe$_3$(BO$_3$)$_4$ [10] by powder neutron diffraction. Our single crystal neutron diffraction on the substituted compositions also clearly indicates the deviation of the magnetic moments from the hexagonal axis. The measured inclination at 2 K corresponds to the averaged in-plane projection of the magnetic moment 0.5(1) μ_B and 0.18(0.5) μ_B for Nd$_{0.9}$Tb$_{0.1}$Fe$_3$(BO$_3$)$_4$ and Nd$_{0.8}$Tb$_{0.2}$Fe$_3$(BO$_3$)$_4$, respectively. Note that the upper limit of 0.5 μ_B for the in-plane projections was reported for TbFe$_3$(BO$_3$)$_4$ estimated from neutron powder diffraction [10].

The small substitution of Nd for Tb leads to the reorientation of the main antiferromagnetic vector **L** from the basal plane towards the hexagonal axis evolving with temperature due to competing magnetic anisotropies of Fe, Nd, and Tb subsystems. The refined *"angular"* magnetic structure at the lowest temperature 2 K reveals noncollinear Fe spin arrangement in the ab plane described by the vectors **B**$_1$ and **B**$_2$ [see Eq. (1)] allowed by symmetry. The "fine structure" determined by the latter could be considered as a weak distortion of the collinear magnetic structure due to the antisymmetric Dzyaloshinsky-Moriya Fe-Fe exchange interaction, which was not observed in the ferroborates until now.

With temperature increase, the "fine structure" fades away and the magnetic structure is described by the usual collinear model. However the deviation θ_L of the antiferromagnetic vector **L** from the c axis still persists and increases with temperature (see Table IV).

It should be noted that average Fe spin values in substituted compounds Nd$_{1-x}$Tb$_x$Fe$_3$(BO$_3$)$_4$ are less than 5 μ_B for the free ion of Fe^{3+}, namely, 3.62(2) μ_B and 3.91(4) μ_B at 2 K, for $x = 0.1$ and $x = 0.2$ correspondingly. Similar spin values were reported for NdFe$_3$(BO$_3$)$_4$ and TbFe$_3$(BO$_3$)$_4$, namely,

4.13(3) μ_B and 4.39(4) μ_B, respectively [8,10]. The exact origin of this discrepancy is not clear yet. Probably it is a result of covalency effect due to the spin density on the ligands [32].

VII. CONCLUSION

The magnetic structures and their temperature evolution were determined in the substituted multiferroics-ferroborates Nd$_{0.9}$Tb$_{0.1}$Fe$_3$(BO$_3$)$_4$ and Nd$_{0.8}$Tb$_{0.2}$Fe$_3$(BO$_3$)$_4$ in the framework of a self-consistent refinement of the neutron diffraction data. The rigid constraints were used in the refinement, implied by the fact that the magnetic order in the rare earth sublattice is induced by the Fe sublattice.

We found in the ground state a complicated noncollinear magnetic order. This structure is characterized by two features: a deviation of the main antiferromagnetic vector **L** from the c axis, allowing us to refer the found structure as an *"angular"* one, and the existence of the additional symmetrized combinations of spin components allowed by a symmetry, namely, vectors **B**$_1$ and **B**$_2$. The latter are determined, in particular, by the antisymmetric Dzyaloshinsky-Moriya Fe-Fe exchange interactions. At higher temperatures for $x = 0.1$ composition we observed a significant increase of the **L** vector deviation from the c axis due to a strong competition of the magnetic anisotropy of the Nd, Tb, and Fe subsystems suggesting the existence of the *"angular"* magnetic structure just below the Néel temperature. However, the low temperature "fine" magnetic structure was not resolved at high temperature and the overall magnetic structure can be described by a simple collinear model.

[1] J. A. Campá, C. Cascales, E. Gutiérrez-Puebla, M. A. Monge, I. Rasines, and C. Ruíz-Valero, Chem. Mater. **9**, 237 (1997).

[2] A. A. Mukhin, A. M. Kuz'menko, V. Yu. Ivanov, A. G. Pimenov, A. M. Shuvaev, and V. E. Dziom, Uspekhi Fizicheskikh Nauk **185**, 1089 (2015).

[3] J. E. Hamann-Borrero, M. Philipp, O. Kataeva, M. V. Zimmermann, J. Geck, R. Klingeler, A. Vasiliev, L. Bezmaternykh, B. Büchner, and C. Hess, Phys. Rev. B **82**, 094411 (2010).

[4] A. M. Kadomtseva, Yu. F. Popov, S. S. Krotov, G. P. Vorob'ev, E. A. Popova, A. K. Zvezdin, and L. N Bezmaternykh, Low Temp. Phys. **31**, 807 (2005).

[5] A. M. Kadomtseva, A. K. Zvezdin, A. P. Pyatakov, A. V. Kuvardin, G. P. Vorob'ev, Yu. F. Popov, and L. N. Bezmaternykh, JETP **105**, 116 (2007).

[6] S. Hayashida, S. Asai, D. Kato, S. Hasegawa, M. Avdeev, H. Cao, and T. Masuda, Phys. Rev. B **98**, 224405 (2018).

[7] P. Fisher, V. Pomjakushin, D. Sheptyakov, L. Keller, M. Janoschek, B. Roessli, J. Schefer, G. Petrakovskii, L. Bezmaternikh, V. Temerov, and D. Velikanov, J. Phys.: Condens. Matter **18**, 7975 (2006).

[8] M. Janoschek, P. Fischer, J. Schefer, B. Roessli, V. Pomjakushin, M. Meven, V. Petricek, G. Petrakovskii, and L. Bezmaternikh, Phys. Rev. B **81**, 094429 (2010).

[9] C. Ritter, A. Vorotynov, A. Pankrats, G. Petrakovskii, V. Temerov, I. Gudim, and R. Szymczak, J. Phys.: Condens. Matter **22**, 206002 (2010).

[10] C. Ritter, A. Balaev, A. Vorotynov, G. Petrakovskii, D. Velikanov, V. Temerov, and I. Gudim, J. Phys.: Condens. Matter **19**, 196227 (2007).

[11] C. Ritter, A. Pankrats, I. Gudim, and A. Vorotynov, J. Phys.: Conf. Ser. **340**, 012065 (2012).

[12] M. Kenzelmann, A. B. Harris, S. Jonas, C. Broholm, J. Schefer, S. B. Kim, C. L. Zhang, S.-W. Cheong, O. P. Vajk, and J. W. Lynn, Phys. Rev. Lett. **95**, 087206 (2005).

[13] T. Goto, T. Kimura, G. Lawes, A. P. Ramirez, and Y. Tokura, Phys. Rev. Lett. **92**, 257201 (2004).

[14] S. Partzsch, J.-E. Hamann-Borrero, C. Mazzoli, J. Herrero-Martin, S. Valencia, R. Feyerherm, E. Dudzik, A. Vasiliev, L. Bezmaternykh, B. Büchner, and J. Geck, Phys. Rev. B **94**, 054421 (2016).

[15] See Supplemental Material at http://link.aps.org/supplemental/10.1103/PhysRevB.99.134439 for sample characterization and magnetic configurations.

[16] J. Rodriguez-Carvajal, Physica B (Amsterdam) **192**, 55 (1993).

[17] S. A. Klimin, D. Fausti, A. Meetsma, L. N. Bezmaternykh, P. H. M. van Loosdrecht, and T. T. M. Palstra, Acta Crystallogr. B **61**, 481 (2005).

[18] P. J. Brown, *Magnetic form factors*, International tables for crystallography Vol. C, edited by E. Prince (Kluwer Academic Publishers, Dordrecht, Boston, London, 2004), Chap. 4.4.5, pp. 454–460.

[19] A. K. Zvezdin, S. S. Krotov, A. M. Kadomtseva, G. P. Vorobev, Yu. F. Popov, A. P. Pyatakov, L. N. Bezmaternykh, and E. A. Popova, JETP Lett. **81**, 272 (2005).

[20] A. K. Zvezdin, G. P. Vorob'ev, A. M. Kadomtseva, Yu. F. Popov, P. Pyatakov, L. N. Bezmaternykh, A. V. Kuvardin, and E. A. Popova, JETP Lett. **83**, 509 (2006).

[21] E. F. Bertaut, Acta Cryst. A **24**, 217 (1968).

[22] J. Rodríguez-Carvajal and F. Bourée, EPJ Web of Conferences **22**, 00010 (2012).

[23] K. P. Belov, A. K. Zvezdin, A. M. Kadomtseva, and R. Z. Levitin, *Orientation Transitions in Rare Earth Magnets* (Nauka, Moscow, 1979) (in Russian).

[24] A. Wills, Physica B **276-278**, 680 (2000).

[25] http://www.cryst.ehu.es/

[26] N. V. Belov, N. N. Neronova, and T. S. Smirnova, Kristallografiya **2**, 315 (1957) [Sov. Phys. Crystallogr. **2**, 311 (1957)].

[27] M. N. Popova, E. P. Chukalina, T. N. Stanislavchuk, B. Z. Malkin, A. R. Zakirov, E. Antic-Fidancev, E. A. Popova, L. N. Bezmaternykh, and V. L. Temerov, Phys. Rev. B **75**, 224435 (2007).

[28] E. A. Popova, D. V. Volkov, A. N. Vasiliev, A. A. Demidov, N. P. Kolmakova, I. A. Gudim, L. N. Bezmaternykh, N. Tristan, Yu. Skourski, B. Buchner, C. Hess, and R. Klingeler, Phys. Rev. B **75**, 224413 (2007).

[29] A. K. Zvezdin, A. M. Kadomtseva, Yu. F. Popov, G. P. Vorob'ev, A. P. Pyatakov, V. Y. Ivanov, A. M. Kuz'menko, A. A. Mukhin, L. N. Bezmaternykh, and I. A. Gudim, JETP **109**, 68 (2009).

[30] A. M. Kuz'menko, A. A. Mukhin, V. Y. Ivanov, A. M. Kadomtseva, and L. N. Bezmaternykh, JETP Lett. **94**, 294 (2011).

[31] A. M. Kuz'menko, A. A. Mukhin, V. Y. Ivanov, A. M. Kadomtseva, S. P. Lebedev, and L. N. Bezmaternykh, JETP **113**, 113 (2011).

[32] V. P. Plakhty, A. G. Gukasov, R. J. Papoular, and O. P. Smirnov, Europhys. Lett. **48**, 233 (1999).